

Discovery of a Large Scale Clumpy Structure around the Lynx Supercluster at $z \sim 1.27^*$

Fumiaki Nakata,^{1,2,3,†} Tadayuki Kodama,^{2,3} Kazuhiro Shimasaku,³ Mamoru Doi,⁴ Hisanori Furusawa,⁵ Masaru Hamabe,⁶ Masahiko Kimura,⁷ Yutaka Komiyama,⁵ Satoshi Miyazaki,⁵ Sadanori Okamura,³ Masami Ouchi,^{8,‡} Maki Sekiguchi,⁹ Yoshihiro Ueda¹⁰, Masafumi Yagi² and Naoki Yasuda⁹

¹*Department of Physics, University of Durham, South Road, Durham DH1 3LE, UK*

²*National Astronomical Observatory of Japan, Mitaka, Tokyo 181-8588, Japan*

³*Department of Astronomy, School of Science, University of Tokyo, Bunkyo-ku, Tokyo 113-0033, Japan*

⁴*Institute of Astronomy, University of Tokyo, Mitaka, Tokyo 181-1500, Japan*

⁵*Subaru Telescope, National Astronomical Observatory of Japan, Hilo, HI 96720, U.S.A*

⁶*Department of Mathematical and Physical Sciences, Faculty of Science, Japan Women's University, Bunkyo-ku, Tokyo 112-8681, Japan*

⁷*Department of Astronomy, Faculty of Science, Kyoto University, Sakyo-ku, Kyoto 606-8502, Japan*

⁸*Space Telescope Science Institute, 3700 San Martin Drive, Baltimore, MD 21210, U.S.A.*

⁹*Institute for Cosmic Ray Research, University of Tokyo, Kashiwa, Chiba 277-8582, Japan*

¹⁰*Institute of Space and Astronautical Science, 3-1-1 Yoshinodai, Sagami-hara, Kanagawa 229-8510, Japan*

Accepted ???. Received ???; in original form ???

ABSTRACT

We report the discovery of a probable large scale structure composed of many galaxy clumps around the known twin clusters at $z = 1.26$ and $z = 1.27$ in the Lynx region. Our analysis is based on deep, panoramic, and multi-colour imaging ($26.4' \times 24.1'$) in $VRi'z'$ -bands with the Suprime-Cam on the 8.2 m Subaru telescope. This unique, deep and wide-field imaging data-set allows us for the first time to map out the galaxy distribution in the highest redshift supercluster known. We apply a photometric redshift technique to extract plausible cluster members at $z \sim 1.27$ down to $i' = 26.15$ (5σ) corresponding to $\sim M^* + 2.5$ at this redshift. From the 2-D distribution of these photometrically selected galaxies, we newly identify seven candidates of galaxy groups or clusters where the surface density of red galaxies is significantly high ($>5\sigma$), in addition to the two known clusters. These candidates show clear red colour-magnitude sequences consistent with a passive evolution model, which suggests the existence of additional high density regions around the Lynx superclusters.

Key words: galaxies: clusters: individual (RXJ 0848.6+4453, RXJ 0848.9+4452) — galaxies: evolution — galaxies: formation — cosmology: large-scale structure of Universe

1 INTRODUCTION

Superclusters are the largest systems of galaxies, composed of multiple clusters of galaxies, extending over 10-20 Mpc (e.g., Bahcall, Soneira 1984; Postman, Geller, Huchra 1988; Quintana et al. 1995; Small et al. 1998). According to the N-body simulations which successfully reproduce the observed filamentary structures at the local Universe (e.g., Peacock et al. 2001), clusters of galaxies at $z \sim 1$ are still in the process of formation (e.g., Moore et al. 1998).

Therefore, clusters of galaxies at this cosmological distance, especially superclusters, are important sites where we can directly see the process of structure formation and evolution and mass assembly to cluster cores.

Despite the importance in the cosmological context, however, only a few superclusters with the scale of >10 Mpc have been identified so far at high redshifts, especially beyond $z \sim 1$ (Connolly et al. 1996; Lubin et al. 2000; Tanaka et al. 2001). The limitation comes largely from the small field of view of large telescopes.

The advent of the Suprime-Cam (Miyazaki et al. 2002), a huge format optical camera with a $30'$ field of view on the prime focus of the 8.2m Subaru telescope, has made it possible for us to view a >10 Mpc region all at once at high redshifts. Kodama et al. (2001) have taken this unique advantage of the Suprime-Cam on Subaru

* Based on data collected at Subaru Telescope, which is operated by the National Astronomical Observatory of Japan.

† E-mail: fumiaki.nakata@durham.ac.uk

‡ Hubble Fellow

Table 1. Log of the observations.

Band	Date	Total Exp.	lim. mag (5σ)	Seeing
<i>V</i>	2000 Nov. 27	96 min	26.78	$\sim 0''.9$
<i>R</i>	2000 Nov. 24	90 min	26.63	$\sim 0''.9$
<i>i'</i>	2000 Nov. 25	30 min	26.15	$\sim 0''.8$
	2001 Mar. 21	30 min		$\sim 0''.8$
<i>z'</i>	2001 Mar. 22	54 min	24.88	$\sim 1''.0$

to map out the large scale structure around the A851 cluster at $z = 0.41$. They have found many filamentary structures and subclumps spreading over 5 Mpc from the dense cluster core, on the basis of photometric redshift (photo- z) analysis, an approach similar to that taken in this *Letter*.

By utilizing the great light-collection power of the Subaru telescope, we now target the most distant supercluster ever firmly identified with spectroscopy: ie., the Lynx supercluster region at $z \sim 1.27$ composed of two known clusters, RXJ 0848.9+4452 at $z = 1.26$ and RXJ 0848.6+4453 at $z = 1.27$, which are spectroscopically confirmed X-ray emitting clusters firstly reported by Rosati et al. (1999) and Stanford et al. (1997). The bolometric X-ray luminosities of RXJ 0848.9 and RXJ 0848.6 are $0.69^{+0.27}_{-0.17} \times 10^{44}$ ergs s $^{-1}$ and $3.3^{+0.9}_{-0.5} \times 10^{44}$ ergs s $^{-1}$, respectively, which are derived with the Chandra observation (Stanford et al. 2001).

Throughout this paper, we use the AB magnitude system (Oke, Gunn 1983). The adopted cosmological parameters are $\Omega_0 = 0.3$ and $\lambda_0 = 0.7$, which gives a physical scale of $8.37h_{70}^{-1}$ kpc arcsec $^{-1}$ at the cluster redshift.

2 OBSERVATIONS, REDUCTION, AND ANALYSIS

2.1 Observations and Reduction

The Lynx field was observed in November 2000–March 2001 in the *V*, *R*, *i'*, and *z'* bands with the Suprime-Cam. Only eight of the ten CCDs of the Suprime-Cam were ready at the time of these observations. Consequently, each image has an FOV of $27' \times 27'$ with a resolution of $0''.2$ per pixel. The log of the observations is given in Table 1.

The images are processed in a standard manner with IRAF and purpose-written software developed by us (Yagi et al. 2002). Flux calibration is performed with photometric standard stars from Landolt (1992) for *V*- and *R*-band, and spectrophotometric standard stars (Oke 1990; Bohlin, Colina, Finley 1995; Bohlin 1996) for *i'*- and *z'*-band. We register the *V*, *R*, and *i'* images with the *z'* image, and match their PSFs to a fixed value, $1''$ (FWHM). Taking an overlapped region for all the images in the four bands, the final area used in our analysis is restricted in a $26'.4 \times 24'.1$ region, which corresponds to $13.3 \times 12.1h_{70}^{-2}$ Mpc 2 at $z = 1.27$. The regions at the edges of the combined image and regions around bright stars were masked and not used in the analysis.

Since the *i'*-band image is the deepest among the four bands with respect to the passively evolving galaxies at the cluster redshift ($i'(5\sigma)=26.15$ mag or $\sim M^* + 2.5$ at $z = 1.27$), we constructed an *i'*-band selected sample using SExtractor v.2.2.0 (Bertin, Arnouts 1996). An area with more than 5 connected pixels with counts over $2.8\sigma_{\text{sky}}$ is identified as an object. Photometry was then performed with a relatively small diameter aperture of $2''$ ($16.7h_{70}^{-1}$ kpc) to keep the signal-to-noise ratios high enough for photo- z use. Galac-

tic extinction is small, $E(B - V) = 0.027$ (Schlegel, Finkbeiner, Davis 1998), and hence neglected. After excluding 411 stellar-like objects, a total of 35143 objects, whose magnitudes are brighter than $i' = 26.15$ (5σ) in the ~ 590 arcmin 2 area, are contained in the final catalog.

2.2 Foreground/Background Subtraction by Photometric Redshifts

Our aim is to map out structures associated with the known twin clusters at $z \sim 1.27$. It is therefore required to remove unassociated galaxies in the foreground and background as much as possible, to maximize the contrast of the structures on the projected sky.

Since spectroscopic measurements for the $\sim 35,000$ galaxies are not practical, we exploit photo- z technique as an observationally efficient method to largely subtract the foreground/background populations. We input the *V**R**i'**z'* magnitudes to the HYPERZ code (Bolzonella, Miralles, Pelló 2000) to get estimated redshifts for all the individual galaxies in our *i'*-band selected sample. This code uses Bruzual & Charlot's (1993) stellar evolutionary code (GISEL98) to build synthetic templates of galaxies for eight star formation histories: an instantaneous burst, a constant star-forming system, and six exponentially decaying SFRs with time-scales of from 1 to 30 Gyr. These models assume solar metallicity and the Miller-Scalo IMF (Miller, Scalo 1979), and internal reddening is considered using the Calzetti et al. (2000) model with A_V varying between 0 and 1.2 mag.

It is ideal to have near-infrared magnitudes as well as optical magnitudes to get better estimates for photo- z 's for galaxies beyond redshift of unity, since the prominent spectral break feature at 4000\AA for old galaxies starts to range out from the optical passbands at $z > 1$ (Kodama, Bell, Bower 1999; Connolly et al. 1997). However, very limited FOVs of current near-infrared imagers on large aperture telescopes (eg., $2' \times 2'$ in the case of Subaru) make it impractical to do near-infrared imaging of such a huge area of our Suprime-Cam field ($\sim 30'$). Nevertheless, by obtaining *z'*-band magnitudes at the longest optical wavelength, whose effective wavelength is about 9200\AA , we can still deal with the galaxies out to $z \sim 1.3$ for photo- z estimates. Our target supercluster is supposed to be located at $z \sim 1.27$, hence the *z'*-band can still just catch the 4000\AA break features. In other words, this target is one of the most distant structures that can be explored by photo- z 's based on the optical imagings alone hence with this huge field of view, except for the rest-UV-selected Lyman break galaxies at exotically high redshifts such as $z > 3$ (eg., Steidel et al. 1999).

By using the best estimate of photo- z of individual galaxies, we select the only galaxies within the range of $1 \leq z_{\text{phot}} \leq 1.35$ to isolate the plausible members associated to the supercluster at $z \sim 1.27$. The number of these photometrically selected candidates for cluster members (hereafter photo- z selected candidates) is 2229. This rather broad range of redshift is intended to ensure that we include the bulk of the cluster population, allowing for the intrinsic errors on photo- z 's. In fact, we find that 14 out of the 16 known true members of the twin cluster, which are confirmed by spectroscopy (Stanford et al. 1997; Rosati et al. 1999), are assigned photo- z 's within the above range. We therefore estimate that the completeness of the members of our method is greater than 80%. For blue cluster members, the estimated photo- z 's tend to be smaller than the true values. It is probably because our photo- z technique misidentifies some blue cluster members as red galaxies at smaller redshifts (Kodama et al. 1999). For this reason, the distribution of $z_{\text{phot}} - z_{\text{spec}}$ is likely to be asymmetric around zero. In

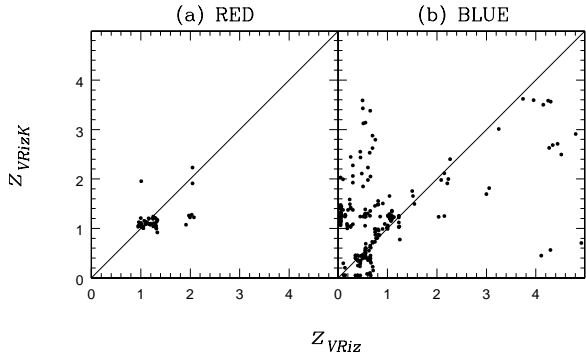


Figure 1. Comparison between the photometric redshifts estimated with and without the K' -band data (Z_{VRizK} and Z_{VRiz} , respectively), for the galaxies in the cl1, cl2 and gr3 down to $K'_{AB} < 23$ (see text for the data). Panel (a) and (b) shows the red and blue galaxies, respectively, separated at the threshold colour (see text).

fact, among the 14 spectroscopically confirmed galaxies, the standard deviation of 5 galaxies with $z_{\text{phot}} > z_{\text{spec}}$ is 0.05, while that of 9 galaxies with $z_{\text{phot}} < z_{\text{spec}}$ is 0.17. Because of this, we take an asymmetric range for photometric members around $z = 1.27$ (ie., $1 \leq z_{\text{phot}} \leq 1.35$). The remaining 2 galaxies are assigned significantly lower redshifts around $z \sim 0.55$. Both of these galaxies have foreground objects near to their images, and the photometry of these member galaxies may be affected by these foreground objects.

To assess our photo- z 's based on the optical data alone (Z_{VRiz}), we compare them to the photo- z 's estimated WITH the K' -band data (Z_{VRizK}), which are available for the selected areas of our fields. It is expected that the photo- z 's at $z \sim 1.27$ with the K' -band have better accuracies since the K' -band neatly covers the longwards of the rest-frame 4000\AA break at this redshift. Here, we use the K' -band imaging data of the 3 regions ($2' \times 2'$ each; centered on cl1, cl2 and gr3 in Figure 2) taken by ourselves with a near-infrared camera CISCO on the Subaru telescope. The integration time of each image is about 30 min and the limiting magnitude is about $K'_{AB} = 23$ (5σ). The comparison is shown in Figure 1. The red and blue galaxies indicate the galaxies redder and bluer respectively than a threshold colour, $(i' - z') = 1.05 - 0.008z'$, which corresponds to the typical colour of the local Sab galaxies (Fukugita, Shimasaku, Ichikawa 1995). The numbers of the red and the blue galaxies plotted in Figure 1 are 48 and 200, respectively. For the red galaxies, we have good match between Z_{VRiz} and Z_{VRizK} , suggesting the accuracy of our optical photo- z 's are reliable enough for these red populations. In fact, the standard deviation, average, and median of $Z_{VRiz} - Z_{VRizK}$ for the red galaxies is 0.15, +0.06, and +0.04, respectively, if we exclude six highly discrepant galaxies with $|Z_{VRiz} - Z_{VRizK}| > 0.5$. For the blue galaxies, however, we see a significant scatter, in particular, we tend to underestimate photo- z 's if we lack the K' -band. Therefore, we must be careful in treating the blue galaxies. In this paper, however, we rely basically on the red galaxies, and hence this is not a big problem.

Given the broad redshift cut for photometric membership, the above photo- z selected candidates should include significant fraction of field contamination which are not associated to the supercluster. Later in § 3, we discuss the level of field contamination in the structures newly found in this study. We stress, however, this photometric selection has already removed the major-

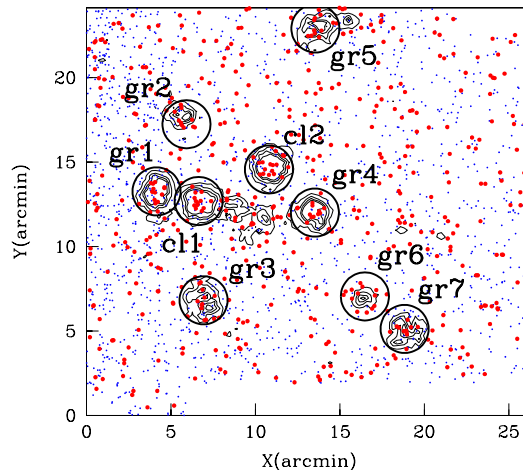


Figure 2. The 2-D distribution of photo- z selected candidates on the sky. North is up, and east is to the left. The large and small dots indicate red and blue galaxies respectively. The contour levels are 2, 3, 4 and 5σ . See the text for details. The radii of large circles are $0.7h_{70}^{-1}$ Mpc at $z = 1.27$.

ity (32914/35143 \sim 95%) of all the foreground/background galaxies while keeping the bulk (\sim 80%) of the cluster members. This essential process has now made it possible for us to unveil the large scale structure possibly associated to the known twin cluster and spread over the entire Suprime-Cam field, which are otherwise embedded in the foreground/background galaxies and invisible.

3 LARGE SCALE CLUMPY STRUCTURE

Figure 2 shows the spatial distribution on the sky of the photo- z selected candidates at $1 \leq z_{\text{phot}} \leq 1.35$. The large and small dots indicate red and blue galaxies respectively defined in §2.2. The numbers of the red and blue galaxies are 575 and 1654, respectively. The positions of the galaxies, X and Y , in the Figure 2 are expressed relative to the bottom-left corner of the Suprime-Cam image. The contours indicate the local surface density of the 'red' photo- z selected candidates calculated from 10 nearest neighbors, corresponding to 2, 3, 4 and 5σ . Here σ corresponds to the scatter (standard deviation) of the local surface density in the case of the random distribution of 575 galaxies over the 590 arcmin^2 field of view, ie., 0.97 arcmin^{-2} . We do not include the blue galaxies here for the following reasons: (1) The accuracy of photo- z is relatively poor for the blue galaxies because of their intrinsically weak 4000\AA feature (§2.2). (2) The red galaxies trace clusters or groups of galaxies more neatly than the blue galaxies due to the morphology(colour)-density relation (Dressler 1980, Dressler et al. 1997). In fact, many authors have exploited this technique and have successfully identified distant cluster candidates in their wide-field data (e.g., Gladders, Yee 2000; Goto et al. 2002). We note that the surface density of the blue galaxies is more than twice larger in the area of $X \lesssim 4.5$ (arcmin) compared to the other area, while the surface density of the red galaxies are nearly the same. This probably comes from the fact that the CCD chips were different between these areas at the time of the observation; in the early phase, the Suprime-Cam consisted of two types of CCDs, SITE (ST-002) and MIT/LL (CCID20). The sensitivities of these 2 CCDs are different especially in the z' -band, where the limiting magnitudes differ by

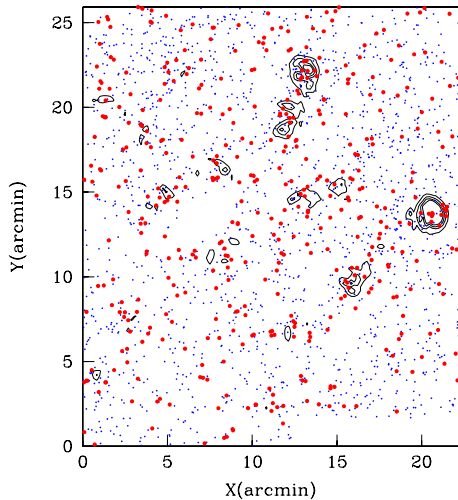


Figure 3. The 2-D distribution of photo-z selected galaxies on the sky in the Subaru Deep Field. North is up, and east is to the left. The symbols and the contour levels are the same as in Figure 2. See the text for details.

~ 0.3 mag. Hence the number of detected galaxies at $X \lesssim 4.5$ with MIT/LL CCD's are increased compared to the other area. Since we count only red galaxies to define local surface density, however, the contours in Figure 2 are not affected by this effect.

In Figure 2, we mark by large circles the areas where the local surface densities of the red galaxies are higher than 5σ above the mean density. The c11 and c12 indicate the 2 known high redshift clusters at $z \sim 1.27$, RXJ 0848.9+4452 and RXJ 0848.6+4453, respectively. We newly find 7 candidates of galaxy clusters or groups, where the local surface density is as large as those of the known clusters (gr1-gr7).

As we noted in § 2.2, our photo-z selected member candidates should include significant amount of field contamination due to the generous criterion for photometric membership ($1 \leq z_{\text{phot}} \leq 1.35$). However, the contrast of our new cluster/group candidates against the general field is always statistically significant. The number density of photo-z selected candidates of red galaxies in the low density ($< 0\sigma$) regions is $2.5 \pm 0.2 h_{70}^2 \text{ Mpc}^{-2}$, while those of the high density regions within the circles of $0.7h_{70}^{-1}$ Mpc radii centered on our cluster/group candidates including the known twin clusters range from $6.3 \pm 2.0 h_{70}^2 \text{ Mpc}^{-2}$ to $11.2 \pm 2.7 h_{70}^2 \text{ Mpc}^{-2}$. To verify the significance of the structures, we present the typical galaxy distribution at $z \sim 1.3$ in the blank field for comparison using the Subaru Deep Field data (SDF; e.g., Furusawa 2002; Kashikawa et al. 2003; Ouchi et al. 2003) in Figure 3. Here we have applied the photo-z using the same passbands ($VRi'z'$) and have extracted only galaxies that fall within $1 \leq z_{\text{phot}} \leq 1.35$, the same criteria that we used for the Lynx cluster field. The contours indicate the surface number density of the red galaxies within this redshift slice and the contour levels are the same as in Figure 2. As shown, only the two areas with $>5\sigma$ peaks are found in the SDF, while 9 such regions are identified in the Lynx field. It is therefore likely that most of the structures that we found in the Lynx field are real. To further strengthen the reality of the large scale structures associated to the twin cluster, we present below the colour-magnitude diagram, radial profile, and the estimate for cluster/group richness for each clump.

Figure 4 shows the $i' - z'$ versus z' diagram for each clus-

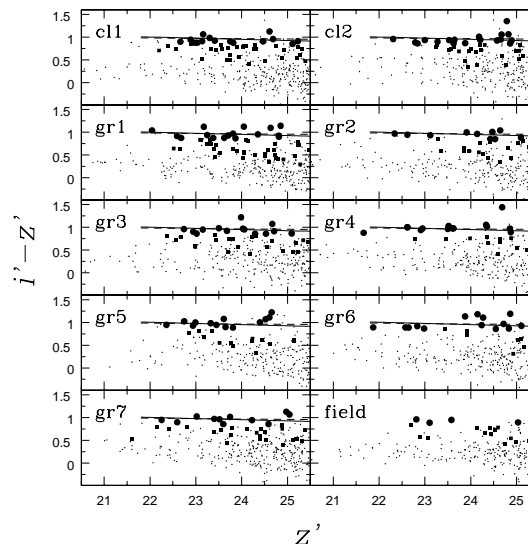


Figure 4. The $i' - z'$ versus z' diagrams of the galaxies in the known clusters (c11 and c12) and our new cluster/group candidates (gr1-gr7). See the text for details.

ter/group candidate including the two known clusters. Galaxies within a circle of $0.7h_{70}^{-1}$ Mpc radius are plotted. The filled circles and the filled squares indicate the photo-z selected candidates of red and blue galaxies, respectively. The small dots show the other galaxies. For comparison, we also show the galaxies randomly selected from the low density ($< 0\sigma$) regions in the bottom right panel of Figure 4. The number of galaxies shown in this panel is the expected number of galaxies within a circle of $0.7h_{70}^{-1}$ Mpc radius calculated from the surface density of galaxies in the Lynx field. The solid line in each panel shows the red sequence of the cluster RDCS 1252 at $z = 1.24$ derived by Blakeslee et al. (2003). We applied an appropriate colour-term correction from HST/ACS filters to Suprime-Cam ones. The dashed line in each panel indicates a predicted colour-magnitude relation at $z = 1.27$ for passively evolving galaxies formed at $z_F = 4.5$ (Kodama, Arimoto 1997), although they are almost identical to the empirically fitted lines (solid lines). Not only in the two known clusters (c11 and c12) but also in our new candidates (gr1-gr7), can we find many red galaxies consistent with the passively evolving galaxies which comprise the red sequences in these diagrams.

We also show the radial profile of each cluster and cluster/group candidate in Figure 5. Only those galaxies brighter than $i' = 26$ are counted because of increasing incompleteness toward fainter magnitudes. Here we subtract the remaining field contamination using the SDF data (see above) from each bin after normalizing counts of field galaxies with referring areas. The averaged surface number densities of all galaxies and the red galaxies are 7.8 ± 7.1 and $0.39 \pm 0.65 h_{70}^2 \text{ Mpc}^{-2}$, respectively, to the same magnitude limit of $i' = 26$. Given the large field of views, the field-to-field variation of the galaxy densities should be averaged over, if present, and hence the accuracy of statistical field subtraction should not be largely affected by this effect. We see a pronounced increase in galaxy density towards the center of most of our cluster/group candidates. The only exception is gr6 that shows no excess of galaxy density at the center. This may be due to the misidentification of the center of the group, or intrinsically non-axisymmetric structure. We combine the profiles

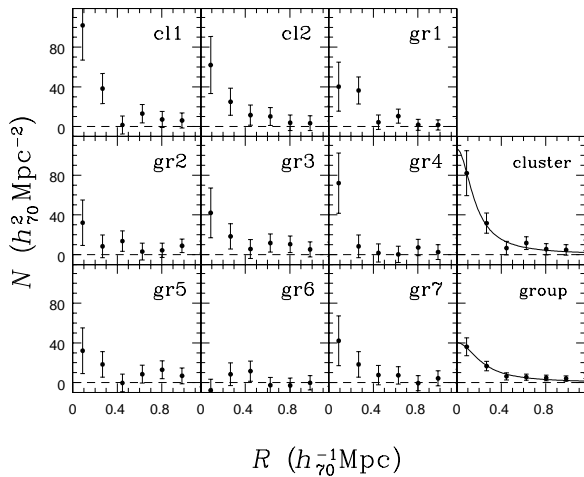


Figure 5. The surface number density of all galaxies as a function of the distance from the cluster center. Cluster and group indicate the combined profiles of the two known clusters and those of our new candidates, respectively, and the best-fitted King’s law profiles are also plotted by the solid lines.

of known clusters and those of our new candidates (groups) separately, and find that both of these combined profiles can be fitted very well with the King’s law profile, $N(r) = N_0(1 + r^2/R_c^2)^{-1}$ (King 1966, 1972), with $R_c = 0.17 \pm 0.02 h_{70}^{-1}$ Mpc (cluster) and $R_c = 0.23 \pm 0.03 h_{70}^{-1}$ Mpc (group), which is consistent with estimations for local clusters (Bahcall 1975).

Table 2 summarizes the properties of the known clusters and the cluster/group candidates. The J2000.0 coordinates of the each cluster/group candidate are given in columns 2 and 3. Columns 4 and 5 show the surface number density of all the galaxies and the red galaxies only, respectively, within a circle of $0.7h_{70}^{-1}$ Mpc radius. We also only use galaxies at $i' < 26$. The remaining field contamination has been subtracted using the SDF data (see above), and the errors indicate the Poisson statistics based on the number of cluster galaxies and that of the subtracted field galaxies. In column 6, we show the estimated richness of each cluster/group candidate, using the $N_{0.5}$ indicator introduced by Hill & Lilly (1991). This indicates the number of galaxies within a 0.5 Mpc radius from the cluster center and within the magnitude range between m_1 and $m_1 + 3$ measured in the R band at $z \sim 0.5$. Since the R band at $z \sim 0.5$ roughly corresponds to the z' -band at $z \sim 1.27$, we can make a direct comparison with their measurements. The cluster richness estimated based on $N_{0.5}$ is 1-2 for c11 and c12, while 0-1 for gr1-gr7 (See Table 4 of Hill & Lilly 1991). Therefore we find that the candidates we newly find are poorer systems than the two known clusters. This is also suggested from deep X-ray data around the Lynx field taken with Chandra (Stanford et al. 2001; Stern et al. 2002). Using the Chandra image in the 0.5–2 keV band, we measure the flux of excess diffuse emission in the circular region around each candidate with a radius of $35''$. The background (the unresolved X-ray background and non X-ray background) is estimated from a surrounding annular region. The result is shown in column 8 of Table 2. Note that gr6 and gr7 are outside of the Chandra field. We cannot detect any significant X-ray excess at more than the 3σ level for our cluster/group candidates except for the two known clusters. It should, however, be noted that the 3σ upper limit luminosity of each region (see column 9 of Table 2) is

comparable to a typical luminosity of nearby groups of galaxies. Thus, the non-detection in the Chandra data does not necessarily imply that the regions we find have unusually low X-ray luminosities compared with their optical richnesses. We argue therefore that our ‘Suprime-Cam imaging + photo- z ’ method is a very powerful technique in finding clusters or groups in the distant Universe even beyond $z > 1$ out to $z \sim 1.3$. We note that this is practically the highest redshift structures of ‘normal’ galaxies that can be traced by optical images with our scheme (bracketing the 4000\AA -break region in the rest frame).

4 SUMMARY

We have presented the results of deep panoramic imaging of the Lynx supercluster field at $z \sim 1.27$ taken with the Suprime-Cam on Subaru Telescope. Our multicolour image covers an area of $26'.4 \times 24'.1$ ($13.3 \times 12.1 h_{70}^{-1}$ Mpc), allowing us for the first time to investigate large scale structure spreading around the known cluster regions at this high redshift. By applying the photometric-redshift technique, we have mapped out the spatial distribution of galaxies near the redshift of the supercluster down to $\sim M^* + 2.5$.

We have newly discovered seven cluster/group candidates. These candidates show red colour-magnitude sequences and centrally concentrated profiles, similar to those of the two known clusters in this field, indicating that they are likely to be real clusters/groups of galaxies around the Lynx supercluster, comprising a large-scale structure over $\sim 13 h_{70}^{-1}$ Mpc scales. The clumpiness of the candidates suggests that they are in early dynamical stages, being in the process of assembly to a massive cluster.

The next key step will be to confirm with deep spectroscopic observations that the cluster/group candidates we discovered in this study are physically associated with one another and forming a real large-scale structure at $z \sim 1.27$. If confirmed, this will be the highest redshift structure of ‘normal’ galaxies ever identified, which will have a large impact on structure formation theories and will bring us invaluable information on the formation and evolution of clusters of galaxies at their early stages.

ACKNOWLEDGMENTS

We thank R. Ellis, R. Bower, M. Balogh, T. Yamada and W. Couch for useful discussion. FN acknowledge the financial support from UK PPARC. FN, TK and MO acknowledge support from Japan Society for the Promotion of Science through its research fellowships for young scientists. SO and TK acknowledge the Daiwa-Adrian Prize 2001 given by The Daiwa Anglo-Japanese Foundation. This work was financially supported in part by a Grant-in-Aid for the Scientific Research (No.15740126) by the Japanese Ministry of Education, Culture, Sports and Science.

REFERENCES

- Aurière, M. 1982, A&A, 109, 301
- Bahcall, N. A. 1975, ApJ, 198, 249
- Bahcall, N. A., Soneira, R. M. 1984, ApJ, 277, 27
- Bertin, E., Arnouts, S. 1996, A&AS, 177, 393
- Blakeslee, J. P. et al. 2003, ApJ, 596, L143
- Bohlin, R. C. 1996, AJ, 111, 1743
- Bohlin, R. C., Colina, L., Finley, D. S. 1995, AJ, 110, 1316
- Bolzonella, M., Miralles, J.-M., Pelló, R. 2000, A&A, 363, 476

Table 2. Properties of the clusters and the cluster/group candidates. Units of right ascension are hours, minutes and seconds, and units of declination are degrees, arcminutes and arcseconds. The local surface densities (Σ , Σ_{red}) given in the table indicate the ones after the remaining field contaminations have been subtracted (see §3 for detail). In the table, $H_0 = 70 \text{ km s}^{-1} \text{ Mpc}^{-1}$, $\Omega_0 = 0.3$ and $\Lambda_0 = 0.7$ are assumed.

	R.A. (J2000.0)	Decl. (J2000.0)	Σ (Mpc^{-2})	Σ_{red} (Mpc^{-2})	$N_{0.5}$	R	$F_X(0.5\text{-}2.0 \text{ keV})^a$ ($10^{-15} \text{ ergs s}^{-1} \text{ cm}^{-2}$)	$L_X(0.5\text{-}2.0 \text{ keV})^a$ ($10^{44} \text{ ergs s}^{-1}$)
cl1	08 48 57.3	+44 52 02.8	20.2 ± 8.3	9.0 ± 2.5	23.6 ± 7.6	1-2	3.8 ± 0.8^b	0.36 ± 0.08
cl2	08 48 34.3	+44 53 52.3	17.1 ± 8.1	10.2 ± 2.7	19.6 ± 7.3	1	4.7 ± 0.5^b	0.44 ± 0.05
gr1 ^c	08 49 11.7	+44 52 37.0	(11.5 ± 6.9)	(9.6 ± 2.6)	(15.4 ± 7.0)	(0-1)	1.0 ± 0.4^d	$< 0.22^e$
gr2	08 49 01.3	+44 56 33.0	9.6 ± 7.9	5.8 ± 2.1	6.6 ± 6.4	0	0.0 ± 0.4^d	$< 0.12^e$
gr3	08 48 57.7	+44 46 09.5	13.4 ± 8.0	8.3 ± 2.4	10.5 ± 6.9	0	-0.2 ± 0.4^d	$< 0.10^e$
gr4	08 48 18.7	+44 51 18.7	7.1 ± 7.8	7.7 ± 2.3	7.1 ± 5.2	0	0.4 ± 0.4^d	$< 0.16^e$
gr5	08 48 18.5	+45 02 13.2	9.5 ± 7.9	8.0 ± 2.4	9.6 ± 6.6	0	0.0 ± 0.3^d	$< 0.10^e$
gr6	08 48 02.0	+44 46 23.1	4.0 ± 7.6	7.1 ± 2.3	4.6 ± 5.4	0
gr7	08 47 48.7	+44 44 27.6	12.1 ± 8.0	5.2 ± 2.0	14.9 ± 6.8	0-1

^a $r = 35''$ aperture

^b quoted from Stanford et al. (2001)

^c The tabulated numbers for gr1 may be significantly affected by the contamination of the blue galaxies in the $X \lesssim 4.5$ (arcmin) region, and hence unreliable.

^d The flux (corrected for the Galactic absorption) and luminosity are given in the rest-frame 0.5–2 keV band. They are converted from the 0.5–2 keV count rate in the observed frame by assuming an optically-thin thermal plasma model at $z = 1.27$ with a temperature of 6 keV and elemental abundances of 0.3 solar.

^e 3σ upper limits

- Bruzual, A. G., Charlot, S. 1993, *ApJ*, 405, 538
 Calzetti, D., Armus, L., Bohlin, R. C., Kinney, A. L., Koornneef, J., Storchi-Bergmann, T. 2000, *ApJ*, 533, 682
 Connolly, A. J., Szalay, A. S., Koo, D., Romer, A. K., Holden, B., Nichol, R. C., Miyaji, T. 1996, *ApJ*, 473, L67
 Connolly, A. J., Szalay, A. S., Dickinson, M., SubbaRao, M. U., Brunner, R. J. 1997, *ApJ*, 486, L11
 Dressler, A. 1980, *ApJ*, 236, 351
 Dressler, A., Oemler, A., Jr., Couch, W. J., Smail, I., Ellis, R. S., Barger, A., Butcher, H., Poggianti, B. M., Sharples, R. M. 1997, *ApJ*, 490, 577
 Fukugita, H., Shimasaku, K., Ichikawa, T. 1995, *PASP*, 107, 945
 Furusawa, H. 2002, PhD Thesis, University of Tokyo
 Gladders, M. D., Yee, H. K. C. 2000, *AJ*, 120, 2148
 Goto, T. et al. 2002, *AJ*, 123, 1807
 Hill, G. J. Lilly, S. J. 1991, *ApJ*, 367, 1
 Kashikawa, N. et al. 2003 *AJ*, 125, 53
 King, I. R. 1966, *AJ*, 71, 1
 King, I. R. 1972, *ApJ*, 174, L123
 Kodama, T., Arimoto, N. 1997, *A&A*, 320, 41
 Kodama, T., Bell, E. F., Bower, R. G. 1999, *MNRAS*, 302, 152
 Kodama, T., Smail, I., Nakata, F., Okamura, S., Bower, R. G. 2001, *ApJ*, 562, L9
 Landolt, A. U. 1992, *AJ*, 104, 340
 Lubin, L. M., Brunner, R., Metzger, M. R., Postman, M., Oke, J. B. 2000, *ApJ*, 531, L5
 Miller, G. E. Scalo, J. M. 1979, *ApJS*, 41, 513
 Miyazaki, S. et al. 2002, *PASJ*, 54, 833
 Moore, B., Governato, F., Quinn, T., Stadel, J., Lake, G. 1998, *ApJ*, 499, L5
 Oke, J. B. 1990, *AJ*, 99, 1621
 Oke, J. B. Gunn, J. E. 1983, *ApJ*, 266, 713
 Ouchi, M. et al. 2003, *ApJ*, 582, 60
 Peacock, J. A. et al. 2001, *Nature*, 410, 169
 Postman, M., Geller, M. J., Huchra, J. P. 1998, *AJ*, 95, 267
 Quintana, H., Reminrez, A., Melnick, J., Raychaudhury, S., Slezak, E. 1995, *AJ*, 110, 463
 Rosati, P., Stanford, S. A., Eisenhardt, P. R., Elston, R., Spinrad, H., Stern, D., Dey, A. 1999, *AJ*, 118, 76
 Schlegel, D. J., Finkbeiner, D. P., Davis, M. 1998, *ApJ*, 500, 525
 Small, T. A., Chung-Pei, M., Sargent, W. L. W., Hamilton, D. 1998, *ApJ*, 492, 45
 Stanford, S. A., Elston, R., Eisenhardt, P. R., Spinrad, H., Stern, D., Dey, A. 1997, *AJ*, 114, 2232
 Stanford, S., A., Holden, B., Rosati, P., Tozzi, P., Borgani, S., Eisenhardt, P. R., Spinrad, H. 2001, *ApJ*, 552, 504
 Steidel, C. C., Adelberger, K. L., Giavalisco, M., Dickinson, M., Pettini, M. 1999, *ApJ*, 519, 1
 Stern, D. et al. 2002, *AJ*, 123, 2223
 Tanaka, I., Yamada, T., Turner, E. L., Suto, Y. 2001, *ApJ*, 547, 521
 Yagi, M., Kashikawa, N., Sekiguchi, M., Doi, M., Yasuda, N., Shimasaku, K., Okamura, S. 2002, *AJ*, 123, 66